STRAIN-DEPENDENT VARIATION OF CRITICAL RESOLVED SHEAR STRESS: A QUANTIZED CRYSTAL PLASTICITY ANALYSIS

THESIS

Presented in Partial Fulfillment of the Requirements for the Bachelors of Science with Honors Research Distinction in the Undergraduate School of The Ohio State University

By

Paul Grant Christodoulou

Undergraduate Program in Materials Science and Engineering

The Ohio State University

2016

Thesis Defense Committee:

Peter Anderson, Advisor

Lin Li (The University of Alabama), Advisor

Maryam Ghazisaeidi, committee member

ABSTRACT

Nanocrystalline (NC) metals are metals comprised of numerous crystals (grains) that are smaller than 100 nm in diameter, on average. They have been an intense focus of research, due to several desirable mechanical properties, including high strength and high wear resistance. The classical Hall-Petch relationship between strength and grain size does not apply, suggesting that the underlying deformation physics is different in NC metals. This study uses the finite element method to explore how a variation in critical resolved shear stress (CRSS) at the nanocrystalline scale affects the macroscopic mechanical response of a NC metal. The model expands on prior work that is predicated on the phenomena whereby a dislocation loop propagates across a grain unimpeded by pinning sites, but is pinned instead by the grain boundary. The nature of this slip event means that each event is accompanied by a quantized change in strain that scales as the inverse of the grain size. The values for strain and the behaviors are mathematically constrained by the critical resolved shear stress, which has a distribution within a polycrystalline sample that is dependent on the size of the grain. This distribution, which is asymmetric, does not change over the previous simulation's runs, and is a key factor to capturing the reversible plasticity in cyclic tension/compression tests. This analysis considers three fundamentally different behaviors: strain hardening, softening, or a mixture of the two. The CRSS increases if hardening is introduced. Hardening also extends the transition from fully elastic to fully plastic behavior and it reduces the recoverable plastic deformation upon unloading. Softening creates an ultimate tensile strength followed by a gradual softening during straining. The clear trends in full width at

half max (FWHM) of the diffraction peaks prove the model is suitable to be used in time-dependent hardening/softening laws compared to experimental creep data for NC Ni. The peak position varies greatly based on the position of the diffraction group in the grain.

ACKNOWLEDGMENTS

I would like to thank Prof. Peter M. Anderson, for helping me through this project, carefully explaining the mechanical behaviors that might be inherent in Nanocrystalline metals. Prof. Lin Li, a graduate of Ohio State, who is now a professor in the Metallurgical and Materials Engineering department at the University of Alabama, for helping me to slowly get a tiny grasp of her work as a PhD student here at Ohio State, who I could consult if I had any problem that I ran into in the QCP model.

Thanks are also in order for Prof. Anderson's group members, notably Xiang Chen, Ryan Smith, David Gutschick, and Kathryn Esham, for assisting me with classes, supercomputer work, and providing me with support through many of my emotional hardships.

I acknowledge the computational support from the Ohio Super Computer Center (Grant No. PAS-0676), and the financial support from the Center of Emergent Materials REU program (under NSF Award Number DMR-1420451).

TABLE OF CONTENTS

LIST OF TABLES

LIST OF FIGURES

CHAPTER 1: NANOCRYSTALLINE METALS AND THEIR MODELS

Nanocrystalline Metal Properties

Nanocrystalline (NC) metals are polycrystalline metals with an average grain size smaller than 100 nm in diameter. They have been an intense focus of research, due to several desirable mechanical properties: (1) high yield and fracture strengths, as shown in Figure 1; (2) an extended elastic-to-plastic-strain transition; (3) large recoverable plastic deformation; and (4) high strain-rate sensitivity [1-8].

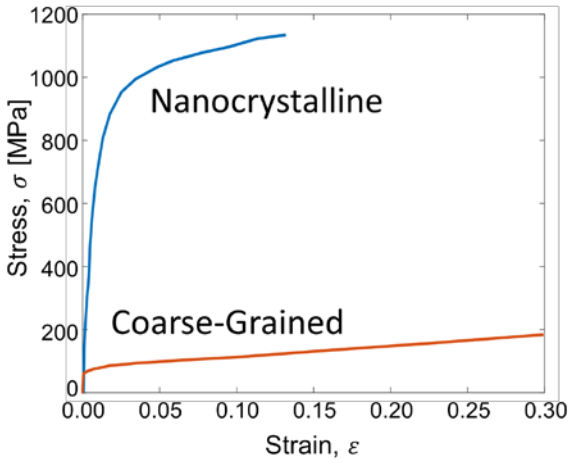

Figure 1: Stress-Strain response of Copper. Adapted from Dao et al [9].

However, NC metals do have limited elongation and toughness, traits that could be considered less than favorable [1-3]. In addition, bulk samples NC can be formed by severe plastic deformation methods that involve high hydrostatic pressures and repeated deformation to refine grains, but ultrafine-grain (UFG), with submicron grain sizes (d=200-500 nm) are the typical results of this grain refinement method. Other methods for bulk formation involve powder metallurgy, and are limited to a select number of alloys [10].

The classical Hall-Petch relationship between strength and grain size, holds for much of the NC regime. This empirical relationship suggests that the yield strength, σ_y, of polycrystals metals increases with decreasing d:

$$\sigma_y = \sigma_0 + kd^{-\frac{1}{2}} \quad (1)$$

where σ_0 is the value as $d \to \infty$, and k is the Hall-Petch coefficient. However, this relationship breaks down at the smallest end of the NC regime, as shown in Figure 2, below, suggesting that the underlying deformation physics is different in NC metals.

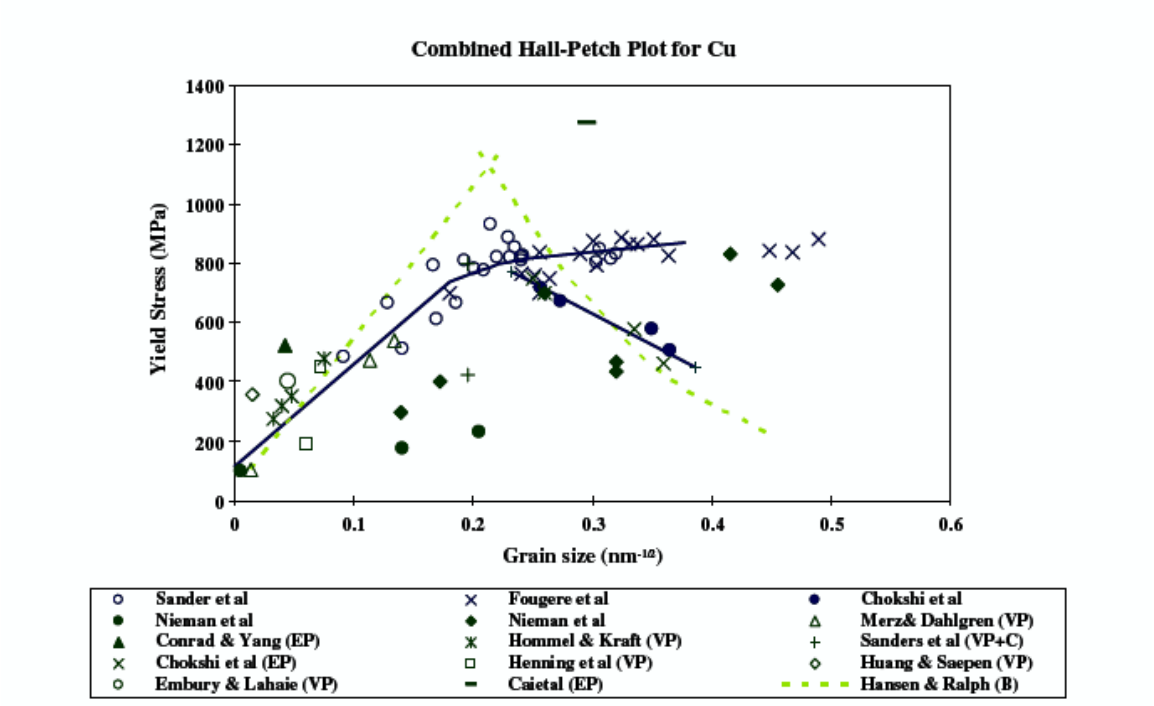

Figure 2: Plot yield strength as a function of grain size (d-1/2) for Cu. Note the breakdown in the Hall-Petch relationship at grain sizes below d=10 nm. Reproduced from [2].

Because of the high density of grain boundaries within NC materials, much of the dislocation activity occurs at the grain boundaries (GBs) [1-6]. The transition from dislocation-mediated deformation to GB sliding or another mechanism is the current

explanation behind the Hall-Petch breakdown that typically occurs on the order of d=10 nm [6].

While we understand the macroscale behaviors of NC metals, there is still incomplete knowledge of their deformation mechanics. As such, computational studies can help elucidate these metals.

Computational Studies of Nanocrystalline Metals

Molecular Dynamics Simulations and Their Predictions

Molecular Dynamics (MD) simulations have provided insight to the mechanisms acting within NC materials. These simulations show us small-scale deformation modes in NC materials, and are categorized into dislocation-mediated or GB-mediated processes. While dislocation activity can be the dominant method of deformation, in the NC regime GBs have a much greater control over the dislocations than in coarse grain (CG) materials [6]. During a slip event, dislocations propagate largely from grain boundary to grain boundary being pinned by GB ledges, as opposed to being pinned within the grain interior by other dislocations as in coarse-grained metals [1-3, 10]. This results in a quantized amount of strain, proportional to $1/d$. This process is shown below in Figure 3, on the following page.

At the onset of a slip event (Figure 3b from simulation), the grain-averaged resolved shear stress reaches a maximum, this maximum value termed the critical resolved shear stress, τ_C, and the dislocation propagates across the grain (Figure 3c), and the grain-averaged plastic strain suddenly increases by an amount $\gamma \propto b/d$, and the resolved shear

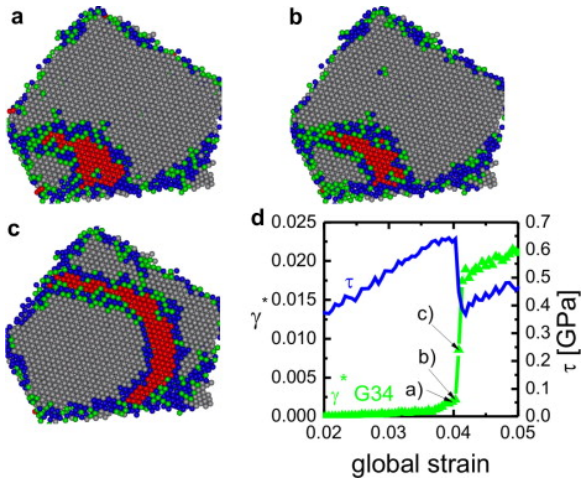

Figure 3: MD simulation of dislocation-mediated deformation in grain, showing a dislocation loop and its associated stacking fault (red atoms) (a) pinned at one side of the grain by GBs, (b) pinned at higher stresses, and (c) breaking away from the pinning sites and shifting unimpededly across the grain. (d) The grain-averaged resolved shear stress, $\boldsymbol{\tau}$, and shear strain, $\boldsymbol{\gamma}$, versus global strain on the polycrystal (taken from [11]).

stress consequently drops (Figure 3d). The reduction in resolved shear stress that coincides with the release in energy via shifting atoms is termed load shedding, $\Delta\tau$.

MD simulations have modeled many dislocation behaviors, but the length and time scales of the model do not apply well to macro-level experimental results [1-3, 12].

Towards the Macroscale: Continuum-Scale Modeling

Continuum models for NC matels fall into one of three categories: (1) two-phase, (2) dislocation slip, or (3) grain-boundary type models.

Two-phase models build on the assumption that GB volume fraction grows as grain size decreases, and thus 'core and mantle' models, such as Fu et al [13], model a grain interior and work-hardened grain boundary zone, and accounts for grain size effects and the breakdown of the Hall-Petch relationship, treating the thickness of the grain boundary, t, proportional to $1/d$ [10, 13]. Wei and Anand have a similar model, where GB are represented as an amorphous second phase surrounding a conventional crystal grain

interior [10, 14]. These studies confirm the transition from grain-interior mechanisms to GB shearing methods occur as d shifts below 50 nm, and indicate that low ductility in NC metals arise from GB shearing and cavitation [10, 13, 14].

Dislocation models work on the idea that dislocations nucleate at the GB, with Asaro et al. and Zhu et al. calculating a critical nucleation stress for all dislocations, proportional to $1/d$, and eventually including variation of grain size within the model [15, 16]. This type of model suggests partial dislocation emission as the dominant deformation pathway, unless a large variation in grain size is present [10]. Bi-modal grain sizes are used as a means to improve ductility in NC metals [1-3].

Finally, grain-boundary type models seek to explore heterogeneous grain-boundary diffusion and sliding to describe reversible plasticity in NC metals. The grain interior deforms by anisotropic elasticity, and the GB have a combination of a high or low diffusivity and sliding viscosity, driving internal stresses that capture reversible plasticity [10, 17].

The Quantized Crystal Plasticity Model and Meso-Scale Modeling

It has been shown that a meso-scale finite element model (FEM), termed the Quantized Crystal Plasticity (QCP) model, captures the behavior experimentally viewed by implementing various principles of MD simulations [1-3]. The QCP model employs conventional crystal plastic formations, which includes an elastic-plastic relation that accounts for texture that has its basis in Schmid's law [11, 18, 19]. The QCP model is predicated on the idea that discrete/quantized changes in strain occur during dislocation slip events as illustrated in Figure 3, by an amount $\gamma \propto b/d$. This finite element model,

termed the Quantized Crystal Plasticity (QCP), captures the enhanced strength, extended elastic-plastic transition, and reversible plastic strength [1-3, 10].

The model itself was defined as a $N \times N \times N$ grain system, where each grain was represented as an eight-node, 3-dimensional cube finite element (C3D8) using ABAQUS/Standard, with constitutive relations typical for large-deformation kinematics crystal plasticity models prescribed in a User-Material (UMAT) subroutine [1-3, 11, 20]. Uniaxial stress is imposed via a constant-magnitude average global strain rate $\dot{\varepsilon}_{global}$ on the top $+Z$ surface in the z-direction, while the x and y faces are free surfaces. Each element is given an initial crystallographic orientation, and represents one face-centered cubic (FCC) grain of Ni. Figure 4 shows this model for N=10, colored with the maximum Schmid factor among the $12\ \frac{1}{2}\langle 110\rangle/\{111\}$ slip systems associated with FCC grains. At the time, a 1000-grains model was determined to balance shear instabilities associated with smaller models and computational cost associated with larger models.

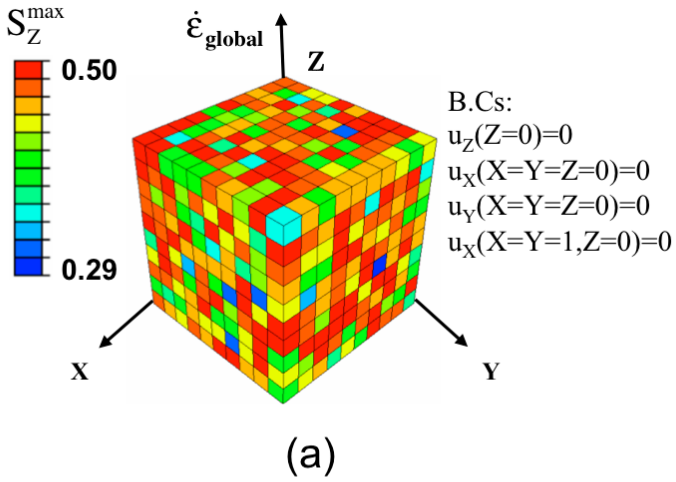

Figure 4: Spatial representation for FEM model with $10 \times 10 \times 10$ grain/elements with C3D8 elements, with the maximum Schmid factor in the z direction color-mapped onto the model, reproduced from [2].

To understand the model, it is necessary to go into greater depth about constitutive frameworks involving large-deformation kinematics. This model is based on Kalidindi et al [21]. An undeformed infinitesimal vector $d\boldsymbol{X}$ is distorted into a vector $d\boldsymbol{x} = \boldsymbol{F}d\boldsymbol{X}$, where the deformation gradient $\boldsymbol{F}$ is

$$\boldsymbol{F} = \boldsymbol{F}^{*}\boldsymbol{F}^{p} \tag{2}$$

where $\boldsymbol{F}^{*}$ and $\boldsymbol{F}^{p}$ are the elastic and plastic parts to this gradient, respectively, thus elastic strain $\boldsymbol{E}^{*}$

$$\boldsymbol{E}^{*} = \frac{1}{2}\left(\boldsymbol{F}^{*T}\boldsymbol{F}^{*} - \boldsymbol{I}\right) \tag{3}$$

where $\boldsymbol{I}$ is the second–order identity tensor The symmetric Piola-Kirchoff stress, the elastic work conjugate to $\boldsymbol{E}^{*}$ at a point is given by

$$\boldsymbol{T}^{*} = \mathbb{C}\boldsymbol{E}^{*} \tag{4}$$

Where $\mathbb{C}$ is the fourth-order compliance tensor, where C_{11}, C_{12}, and C_{44} are independently defined. $\boldsymbol{T}^{*}$ is related to Cauchy stress $\boldsymbol{T}$ by

$$\boldsymbol{T}^{*} = \det(\boldsymbol{F}^{*})\,\boldsymbol{F}^{*-1}\boldsymbol{T}\boldsymbol{F}^{*-T} \tag{5}$$

In the QCP model, the Caushy stresses in the x and y directions is 0. The time evolution for $\boldsymbol{F}^{p}$ is

$$\dot{\boldsymbol{F}}^{p} = \boldsymbol{L}^{P}\boldsymbol{F}^{P} \tag{6}$$

where $\boldsymbol{L}^{\boldsymbol{P}}$is the velocity gradient calculated by

$$\boldsymbol{L}^{P} = \sum_{a} \dot{\gamma}^{\alpha}\boldsymbol{S}_{0}^{\alpha}\,, S_{0}^{\alpha} = \boldsymbol{s}_{0}^{\alpha} \otimes \boldsymbol{m}_{0}^{\alpha} \tag{7}$$

where the active slip direction s_0^{α} and slip plane normal m_0^{α}, and thus $\boldsymbol{S}_0^{\alpha}$ represents one of the 12 $\langle 110\rangle/\{111\}$ slip systems, and thus $\alpha = 1 - 12$. The plastic shear rate $\dot{\gamma}^{\alpha}$ shown in Equation (7) is a function of resolved shear stress τ^{α} and critical resolved shear stress τ_C^{α}

$$\dot{\gamma}^{\alpha} = \hat{\dot{\gamma}}^{\alpha}(\tau^{\alpha}, \tau_C^{\alpha}) \tag{8}$$

where τ^{α} is defined as

$$\tau^{\alpha} = \boldsymbol{s}_0^{\alpha}(\boldsymbol{F}^{*T}\boldsymbol{F}^{*}\boldsymbol{T}^{*})\boldsymbol{m}_0^{\alpha} \tag{9}$$

essentially accounting for the random Schmid factors shown in Figure 4 above. The value τ_C^{α} is called the critical resolved shear stress, and in the previous QCP models, is a material property assigned to each individual grain at the onset of the model, and remains constant throughout the duration of the simulation. One important factor of this model was that the τ_C^{α}, further denoted τ_C for brevity, within the grains should be heterogeneous in order to capture the behavior of the experimental results. *Yuan et al*, with a similar meso-scale model, indicated that a possible source of this heterogeneity is the size of the pinning site, which in NC metals is the distance between two points on the grain boundary [8]. This heterogeneity of hardness proved necessary to capturing the reversible plasticity upon unloading [1, 2, 11] and a gamma-type distribution, as in Equation (10), used in conjunction with the QCP model created an acceptable fit to experimental data.

$$\rho(\tau_C, k, \theta) = (\tau_C - \tau_{min})^{k-1}\frac{\exp(-(\tau_C - \tau_{min})/\theta)}{\Gamma(k)\theta^k} \tag{10}$$

Where k is the shape parameter, τ_{min} is a value below which $\rho(\tau) = 0$, and θ is a scale parameter. This distribution is skewed to favor a low average, where most grains are plastically soft, but with a large tail including some very plastically hard grains. A symmetrical distribution was also tested, but is not the basis of the current study.

The discrete jumps in strain are represented by:

$$\Delta\gamma^{p} = \gamma_{target}s_0^{\alpha} \otimes m_0^{\alpha} \tag{11}$$

where $\Delta\gamma^p$ is the change in plastic strain in the active slip direction s_0^α and slip plane normal m_0^α, and γ_{target} is defined by

$$\gamma_{target} = \frac{A_s b}{V_g} = g\frac{b}{d} \tag{12}$$

where $A_s$is the cross sectional area, and V_g is the grain volume, and b is the Burgers vector magnitude. Thus, g becomes a geometric factor, with a maximum value of ~1.2 for the current cubic elements, and d is the length of each side.

Here, the model varies from Kalidindi et al. [2, 3, 11]. The plastic shear strain on the 12 slip systems is modified from Equation (40) in Kalidindi et al. [21], and satisfies Equation (8) by

$$\dot{\gamma}^\alpha = \begin{cases} \dot{\gamma}_0 \left|\frac{\tau^\alpha}{R\tau_c}\right|^{\frac{1}{n}} sign(\tau^\alpha) & inactive\ slip \\ \dot{\gamma}_0 sign(\tau^\alpha) & active\ slip \end{cases} \tag{13}$$

where active slip occurs when $|\tau^\alpha| \geq \tau_C$. Active slip is complete when $\gamma^{p,\alpha}$ increments by γ_{target}, in spite of the fact that $|\tau^\alpha|$ decreases below τ_C due to load shedding. The coefficient R is chosen such that $\dot{\gamma}^\alpha < 10^{-20}\dot{\gamma}_0$, reinforcing the numerical inactivity condition. The chosen power-law constant n, will change the value of R. The slip rate $\dot{\gamma}_0$ must be greater than 10 times that of the global strain rate $\dot{\varepsilon}_{global}$, simulating relatively instantaneous slip. In the case where $\dot{\varepsilon}_{global} \leq 1 \times 10^{-3}/s$, a value of $\dot{\gamma}_0 = 2 \times 10^{-2}/s$ is acceptable. For the purposes of this model, n=0.1 was chosen to ensure stability.

There is, additionally, a *propagation condition* setting a lower bound on τ_C and an upper bound on γ_{target}, predicated on the fact that τ^α does not change during a slip event,

guaranteeing that there is enough stress to continue the expansion of the dislocation loop. Thus, the load shedding amount must be constrained to

$$\Delta\tau = c\Delta\tau^{Eshelby} = cM\gamma_{target}; M = \mu\frac{7-5\nu}{15(1-\nu)} \tag{14}$$

for ellipsoidal regions, where μ is the elastic shear modulus and ν is Poisson's ratio. An additional parameter, c is introduced to account for the cuboidal grain elements such that

$$\tau_C \geq cM\gamma_{target} \text{ or } \gamma_{target} \leq \tau_c/cM \tag{15}$$

In the QCP simulation, $\gamma_{target}$is then constrained so that it is the minimum value of Equations (12) and (15) such that

$$\gamma_{target} = \min\left(\frac{\tau_C}{cM}, 1.2\frac{b}{d}\right) \tag{16}$$

where τ_C is assigned as mentioned above.

Additional comparison to the previous model will be included within the body of this work.

Temporal Variation of Critical Resolved Shear Stress

Yuan et al. included a temporal variation of critical resolved shear stress, indicating that strain hardening was present even with a constant critical resolved shear stress, but a randomized value (selected from the distribution that the model had originally been designated) was selected and assigned to the slip system in the grain provided a greater strain-hardening response [8]. Strain hardening is also present in the QCP model, but, as previously mentioned, the grains only have one critical resolved shear stress, representing the minimum value. This would shift the expected τ_C distribution in favor of the softer grains.

This study uses the finite element model (FEM) to explore how a shear-dependent evolution in critical resolved shear stress at the nanocrystalline scale affects the macroscopic mechanical response of NC Ni, to further develop the theory on hardness heterogeneity.

CHAPTER 2: TENSION TESTING

Motivation

The motivation of this test was to expand Li's model, and see its effects on a simple tension test, isolating elastic-plastic transition, and strain hardening. Within a physical model, softening could arise from dislocation annihilation over time, due to temperature effects, or the consumption of weak depinning sites. Hardening can come from many sources, from interactions with neighboring grains that have slipped creating additional stress on the grain to dislocations pileups at the grain boundary, the creation of extra depinning ledges, etc.

Implementation

The current model is identical to Lin's previous model, except for two variations: the integration points in each element have been reduced from 8 to 1 per element (C3D8R), and the value of τ_C for each element alters after a slip event completes. Because fitted data was available for NC Ni, Table 1 on the following page summarizes the utilized for NC Ni with an average grain size of d=30 nm. The model was strained in tension at a rate of $\dot{\varepsilon} = 10^{-3}$/s for 50 seconds.

Table 1: Summary of Parameters for QCP model for NC Ni, d=30 nm [1, 2, 11].

Ni Elastic Moduli [22] (GPa)	C_{11}: 246.5	C_{12}: 147.3	C_{44}: 124.7
Ni Polycrystalline Moduli (GPa)	E =236.5	μ =94.7	hourglass:473.5
Poisson's ratio	ν =0.276		
Burgers vector (nm)	b:0.25		
Crystal Texture	Random with average maximum Schmid factor = 0.45		
Ave. grain size d (nm)	30		
Macro strain rate (1/s)	$\dot{\varepsilon} = 10^{-3}$		
Crit. stress distribution (MPa):	k = 1 θ = 840 $\tau_{c(min)}$ = 210		
Quantized plastic strain: γ_{target} = min(τ_c/60, 1.2 b/d)	$\gamma_{target\ min}$ = 4.7x10^{-3} $\gamma_{target(max)}$ = 6.0x10^{-3}		
Computational Parameters	$\dot{\gamma}_0$ (s^{-1}): 2x10^{-2}	n: 0.1	$\Delta\tau$: $\gamma_{target,max}/\dot{\gamma}_0$
	M=50 MPa	c=1.2	

The part was reduced to a reduced-integration-point model with an hourglass stiffness of 473.5 GPa, which was the number suggested by Abaqus based on the shear modulus μ [23], and the number that produced the closest agreement between reduced and full integration point simulations. The user-defined material (UMAT) subroutine was modified to include the variation of τ_C.

The model considers three fundamentally different behaviors that might occur within the material: strain hardening, softening, or a mixture of the two. This is done by changing the value of τ_C after each slip event in a grain occurs. Within the model, the value can either increase or decrease. When a slip event occurs, the grain experiences load shedding accompanied by a discrete strain. After this slip event is complete, the value for τ_C changes. Monotonic hardening or softening in the system is modeled with a monotonic increase (I) or decrease (D) in τ_C, respectively, while a mixture rule was simulated by randomly (R) selecting a value from the γ distribution in Equation (10). Table 2 summarizes this change, including (C), which is the constant τ_C model. Figure 5 shows

the τ_C value during the course of one slip event. While τ_C is the value that changes, it is easiest to show the model's effects on one grain, so Figure 5 primarily is intended to show the timing and nature of the change in τ_C.

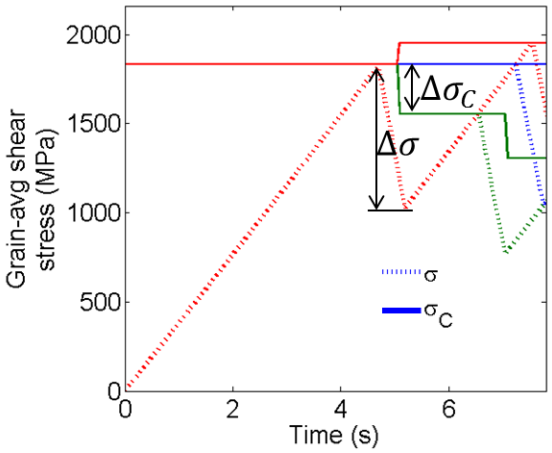

Figure 5: Stress in a single grain, with the change in critical resolved shear stress indicated by the critical stress.

Table 2: Summary of the variations attempted on the QCP model.

Case	Change
I	Increase 300 MPa
D	Decrease 10%
R	Random
C	No Change

The strain hardening was modeled in Case I, where τ_C increases by 300 MPa, which is about half the expected magnitude of load shedding $\Delta\tau$ in all most grains, calculated using Equations (14) and (15), with the computational parameters listed in Table 1. The magnitude of $\Delta\tau$ in most grains is ~600 MPa, except in cases where τ_c is less than this value. There was no computation error that could result from increasing τ_C arbitrarily. While it was feasible to decrease τ_c, because of the load shedding $\Delta\tau_c$ must be less than $\Delta\tau$ in order to have a convergent simulation. This relationship can be seen below:

$$\Delta\tau_c = \tau_{c,old} - \tau_{c,new} < \Delta\tau \tag{17}$$

The models for random τ_c assignment and stress softening were thus more challenging to implement. In the strain softening case, Case D, τ_c decreases 10% of the current τ_c, until it is equal to $\Delta\tau$. Case R, the random case, assigned a value from a gamma distribution (Equation (10)), which is used to initially assign τ_C where the shape factor k=1, and θ follows Equation (18).

$$\theta = \tau_{c,mean} - \tau_{c,\min} = 1050 - 210\ MPa \tag{18}$$

This gives the equation

$$\rho(\tau, 1, 840) = \frac{\exp(-(\tau - 210)/840)}{\Gamma(1)840} + 210 \tag{19}$$

This specific distribution corresponds to the distribution that created fit best with experimental data from 30 nm-diameter electrodeposited Ni [1, 2]. The shape of the distribution is quite asymmetric, as can be seen in Figure 6.

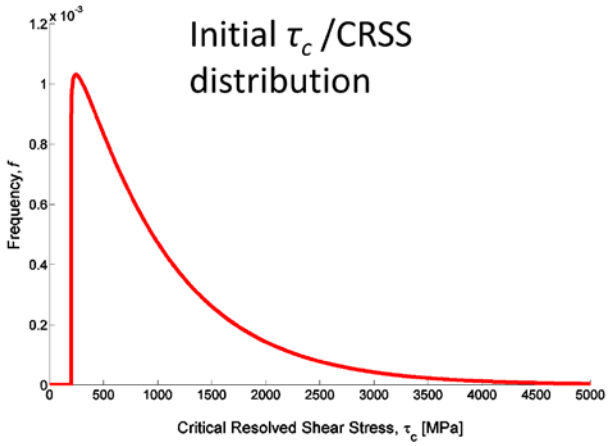

Figure 6: Critical Resolved Shear Stress Gamma Distribution.

The random-assignment method is much like one in another study [8], but uses a different τ_c distribution, and each grain has one assigned value for τ_C on all slip systems, representing the minimum resolved shear stress necessary to cause a slip event.

The final case, Case C, is the control case, which is identical to the original QCP model, except for the reduced-integration alteration. Note also that the propagation affected the random value assignment, such that if $\tau_C^{assigned} < \tau_C^{current}$, and $\Delta\tau_C > \Delta\tau$ or $\tau_C^{assigned} < \tau_C^{min}$, then the $\Delta\tau_C$ became ½ $\Delta\tau$ or $\tau_C^{assigned}$ became instead τ_C^{min}. This limited the amount that a crystal could decrease by.

Results/Discussion

The primary goal was to confirm that there was an effect within the simulation. Figure 7, on the following page, shows the change in critical resolved shear stress distribution over the course of the 2500 frames.

The associated time and average values for each frame in each case is listed in Table 3 below. As is visible in each case, the critical resolved shear stress does indeed change over time. Cases I and R both have an upward shift in τ_c.

Table 3: Average τ_c value at specific time frames in the model.

Table 4: Average τ_c value at specific time frames in the model.

Frame	Time (s)	Case D	Case I	Case R
1	0.010	1050.7	1050.7	1050.7
501	9.995	1047.7	1086.9	1142.5
1001	19.99	1041.8	1152.5	1273.1
1501	29.99	1035.8	1223	1387.4
2001	40.00	1031	1295.1	1485.6
2501	50.00	1027.1	1367.2	1573.0

The specific method through which Case R was implemented contributed to the overall similarity with Case I. Because the first grains to slip were the grains with the lowest τ_c value, it is expected that a randomly assigned value would be greater than the current value, particularly because the softest grains would slip first, and the propagation condition was in effect. In Case D, very little change can be seen. Because of the conditions, only grains above 600 MPa could experience a large decrease. As such, τ_c decreases most for grains within the middle of the distribution, around 600-2000 MPa.

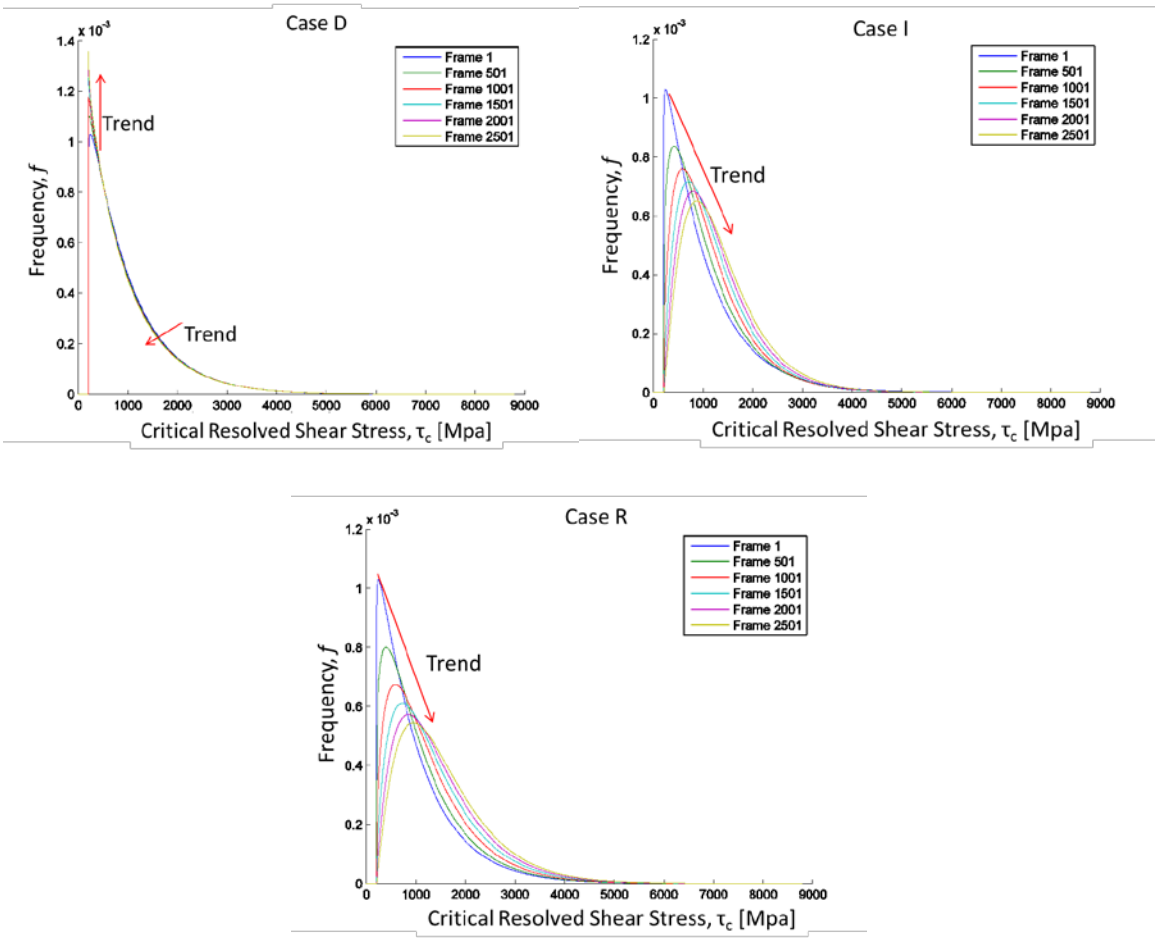

Figure 7: τ_C distribution over the course of the simulation for (a) increasing (b) decreasing, and (c) random τ_C.

The stress-strain response for each of these cases is shown in Figure 8, below. The stress-strain response is expected: cases I and R have a larger elastic-plastic transition and greater strain hardening, while case D shows decreases transition and strain hardening. Strain hardening for random change in hardness was also found in Yuan et al. [8]. Also, as expected, there is no change in the elastic/linear regime: all cases are identical until the first slip event occurs at the onset of the elastic-plastic transition. Case D has a comparable elastic-plastic transition to the control.

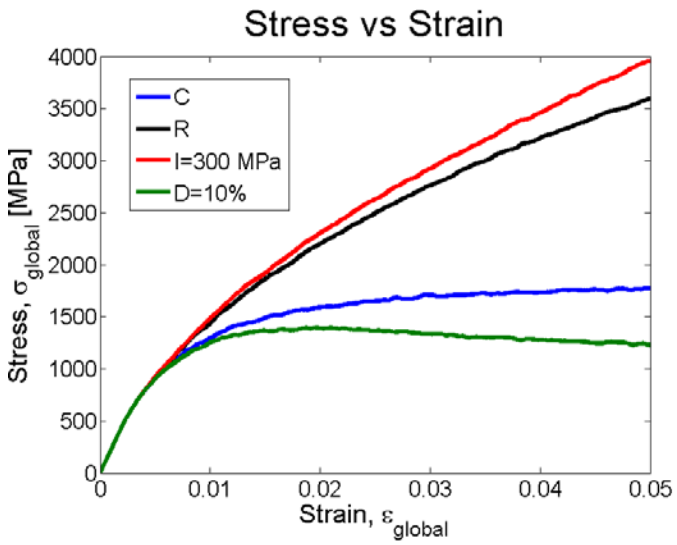

Figure 8: Stress-Strain response of the control and three altered hardness cases.

Case D appears to exhibit an ultimate tensile strength, followed by a negative slope. This negative slope could be due to the softening of the mid-range grains, which would not begin to slip until many of the softer grains had slipped many times.

The number of slip events that occurred within each of the 1000 elements up to 47.98s is summarized in Table 5, below.

Table 5: Number of slip events at 47.98 seconds, just prior to the end of the simulation.

Case	Average	Max
C	2.116	20
D	2.215	23
I	1.595	5
R	1.641	6

These results parallel the strain hardening behavior, that is, the least amount of strain hardening that occurs, the lower the number of slip events. In Case D and Case S/C_0, the same grains had the most activity, as can be seen in the spatial view model in Figure 9. These grains are the softest grains within the model, and so are the easiest to deform. In the hardening and random cases, Case I and R, the activity is more diffuse and lesser in number. The grains that have the most activity are not the same as in the constant and decreased τ_C cases, because the softest grains were the first to harden, and were subsequently less active in terms of slip events.

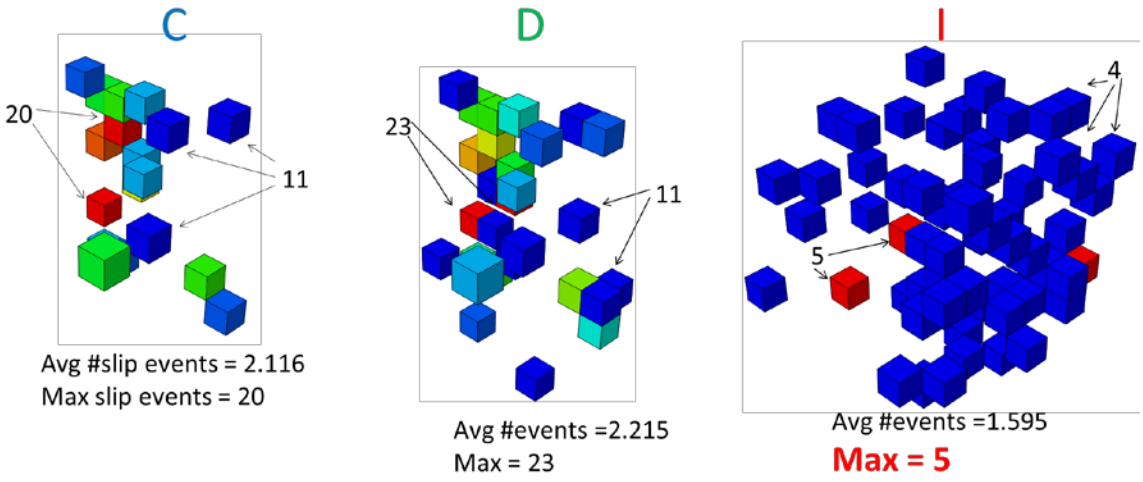

Figure 9: Physical position of all elements that have more than 10 slip events within the model the coloring is based on the scale used in Figure 4. It is worth noting that the yellow grain in case D corresponds to 20 slip events.

Comparing the fitted constant simulation to the other cases, it is clear that any behavior would have to be slight, or balance moderate amounts of hardening and softening.

CHAPTER 3: CYCLIC TESTING

Motivation

The heterogeneity of the critical resolved shear stress τ_C in the $10 \times 10 \times 10$ element model was necessary in order to capture the curvature of the response, as well as the reversible plastic deformation. Figure 10 shows the fits from the previous model. With an with a uniform τ_C distribution, no reverse plasticity is observed.

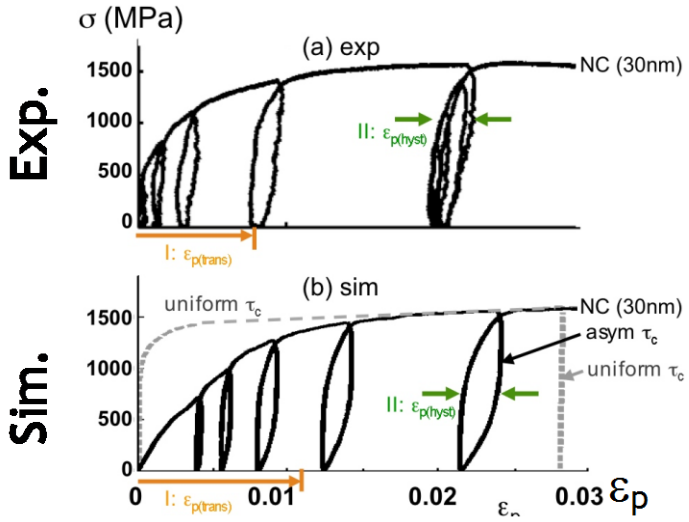

Figure 10: Cyclic stress strain of both experimental and QCP simulation NC Ni, to illustrate the importance of asymmetry in the critical resolved shear stress distribution (taken from [24]). The area between the green arrows will hereafter be referred to as hysteretic strain width.

Additionally, this asymmetrical gamma distribution was tested to match experimental diffraction data, shown in Figure 11, on the following page.

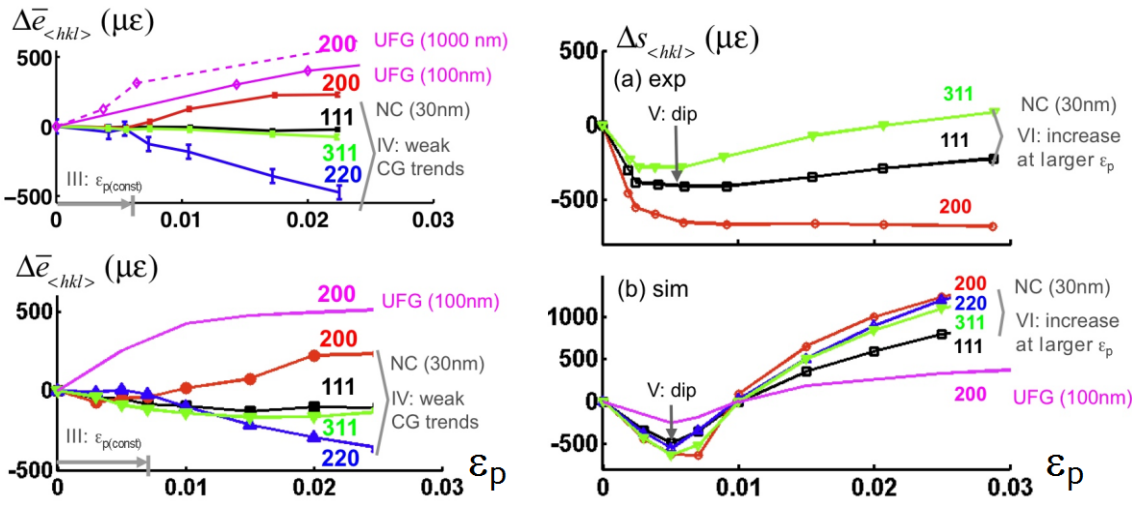

Figure 11: Experimental (top) and simulated (bottom) diffraction data, showing the peak position on the left, and the full width at half maximum (FWHM) of the peaks on the right. Reproduced from [24].

Diffraction data represents the shift from the center peak—that is the amount of internal strain in the model, resulting from the overstretching of soft grains and understretching of hard grains. This behavior is thought to contribute to the reversible plasticity behavior. Additionally, diffraction behavior can show strain development over time, to indicate small-scale behavior. For instance, as the FWHM of each peak increases, this indicates that the grains in a particular diffraction group have grown more heterogeneous in terms of plastic strain. This data can determine the behavior of each particular diffraction group. From previous testing, we know that the ⟨220⟩ direction is hard, and thus when the part is unloaded, this grain experiences tension in the z direction, and is thus shifted in compression in the transverse direction, so on a diffraction plot, this direction typically shifts in compression. It is compensated in part by the ⟨200⟩ direction, which typically shifts transversely in tension, shown in Figure 11, and explained pictorially in Figure 12.

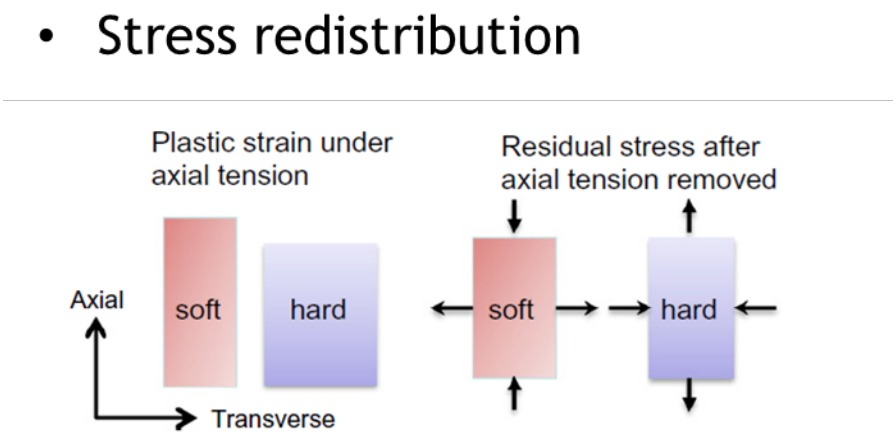

Figure 12: Stress redistribution in locally soft and hard grains, accounting for diffraction behavior in the diffraction groups and physically hard/soft grains. Taken from [24].

The goal of this portion of the model is to determine if any hardening/softening behavior is more promising for fitting than the current behavior.

Implementation

For cyclic strain, the model begins in compression to -0.0056 plastic strain, then shifts to tension loading, followed by unloading/reloading at a plastic strain of 0.005, and at regular intervals of 0.005 to 0.025 global plastic strain. This cycle continues until the 150 seconds are complete. In addition to the previous I, C, R, and D cases, a second monotonically increasing (I) case was introduced where the value increased by 1% after each slip event. After the initial cyclic data, the same test was completed 10 times for each case (I=1%), (D=10%), (R), and (C). In each case, the only change was the orientation of the grains. The 1000 previously assigned orientations were shuffled around the model, but each specific grain still began with the same τ_C as in previous cases. The average displacement and standard deviation of residual plastic strain was cataloged such

that it simulated diffraction data. This value was taken at every unloaded point, or anytime there was no stress on the system.

The previous data had simulated precompression because the diffraction data had a clear reversal in slope near 0.5% strain, as in Figure 11, so the precompression simulates an initial residual stress from processing, possibly a heat treatment effect.. For a comparison of diffraction data, a tension-only test was completed with the same strain rate magnitude and positive unloading/reloading plastic strain.

Results/Discussion

Stress/Strain

The amount of reversible plasticity is affected by all modifications to τ_C. Figure 13, below, shows the cyclic stress-strain response of the chosen cases, based on the initial set of crystal orientations. What is notable about this response is that hysteretic strain width is almost negligible in the most severe of hardening cases. This confirms the previous findings that a heterogeneous distribution of plastically soft and hard grains was necessary in order model the reversible plastic deformation behavior.

A graph of the strain width, shown in Figure 14, shows that the amount of reversible plasticity is less for all cases beyond the static τ_C control (C) case. Obviously, if the current model appropriately simulates the mechanisms involved, there is not a great deal of hardening that can occur before the model no longer captures the hysteretic behavior. Because of this, the second, less drastic, Case I (1%) was introduced, and used for the diffraction data.

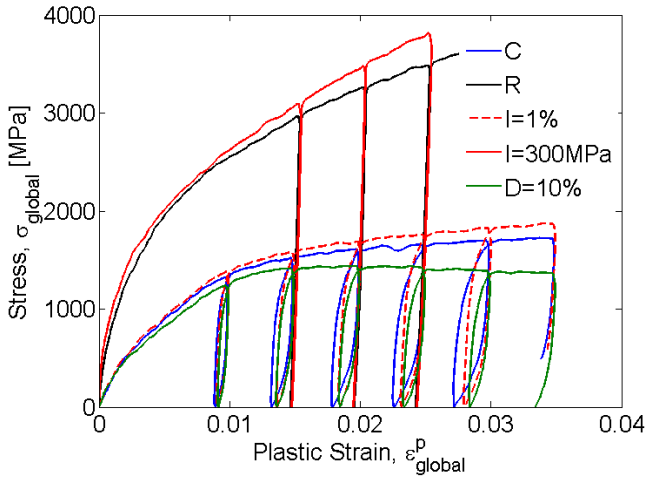

Figure 13: Cyclic stress-strain response of the constant τ_C and the chosen modifications.

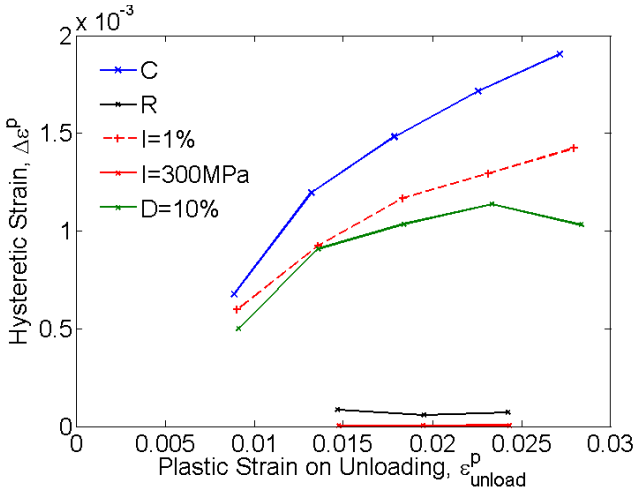

Figure 14: Plot of maximum hysteretic strain width as a function of plastic deformation upon unloading.

Diffraction Data

As explained in the implementation section, in order to get a statistically-significant analysis for the diffraction, 10 identical cases with a different distribution of Euler angles were averaged together. However, of those ten, two of the simulations did not converge in all 4 τ_C cases. The diffraction data averages of 7 of the remaining 8 cases (Euler sets 1-7) can be seen below in Figure 15. Note that the FWHM averages, while standard

deviations, were averages of the standard deviation of each case, not the overall deviation from all of the cases. Between each of the 8 cases, the variation in average was great, but the standard deviation of the grains had a consistent shape in each case.

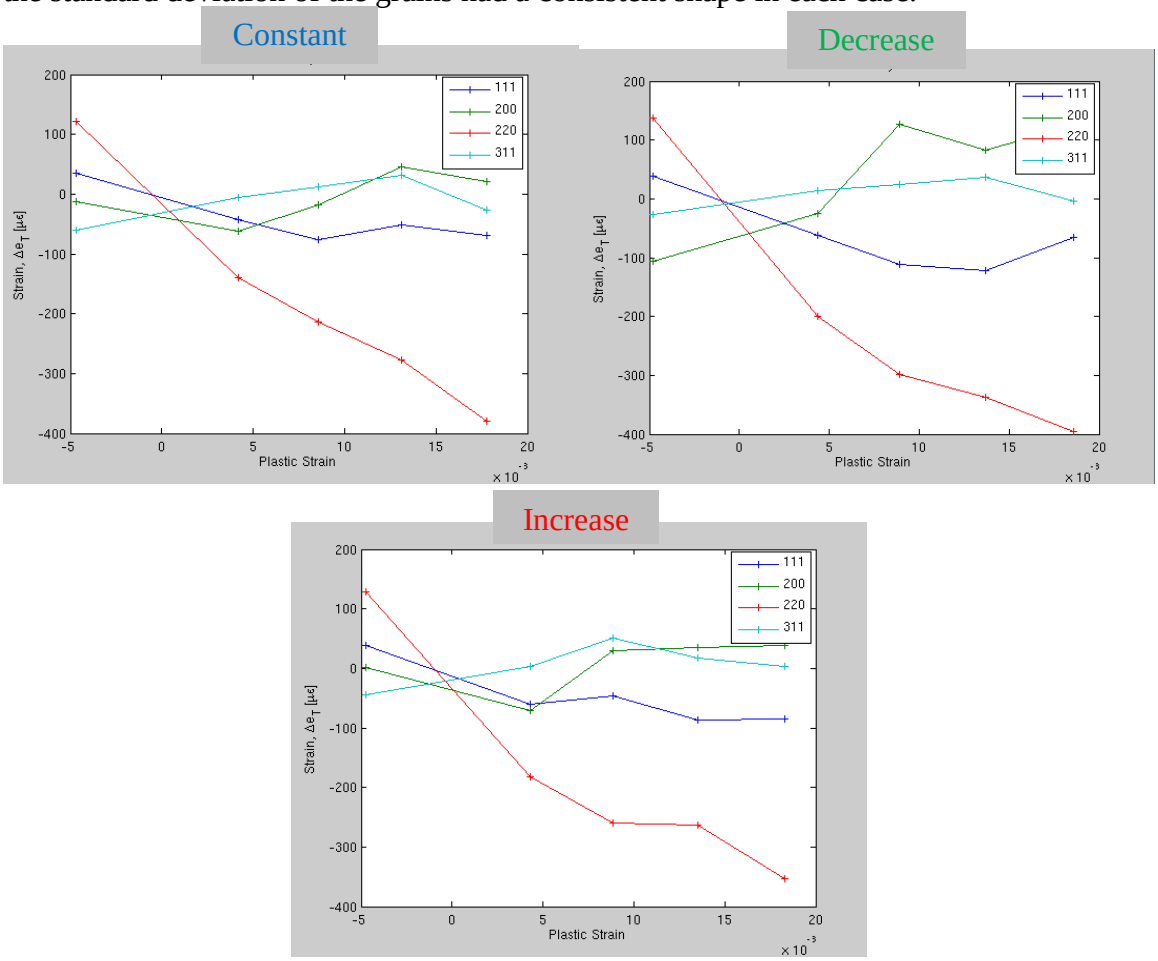

Figure 15: Diffraction data averaged for the first 7 cases (case number 8 and 10 did not converge) for the constant, decrease, and increase 1% case.

One important factor for this variation appeared to be the location of the diffraction peak on the interior vs the exterior. Figure 16 illustrates the same data for interior grains only. Because of the size of the simulation, the number of external and internal grains is nearly parity at 488 external grains and 512 internal grains, any shift in the orientations could potential shift the grain averages significantly, particularly in the case of the soft ⟨200⟩

slip direction. A larger number of iterations would likely prove useful for determining behavior independent of the material, as well as having a data point at the expected crossover point, and 0% global plastic strain.

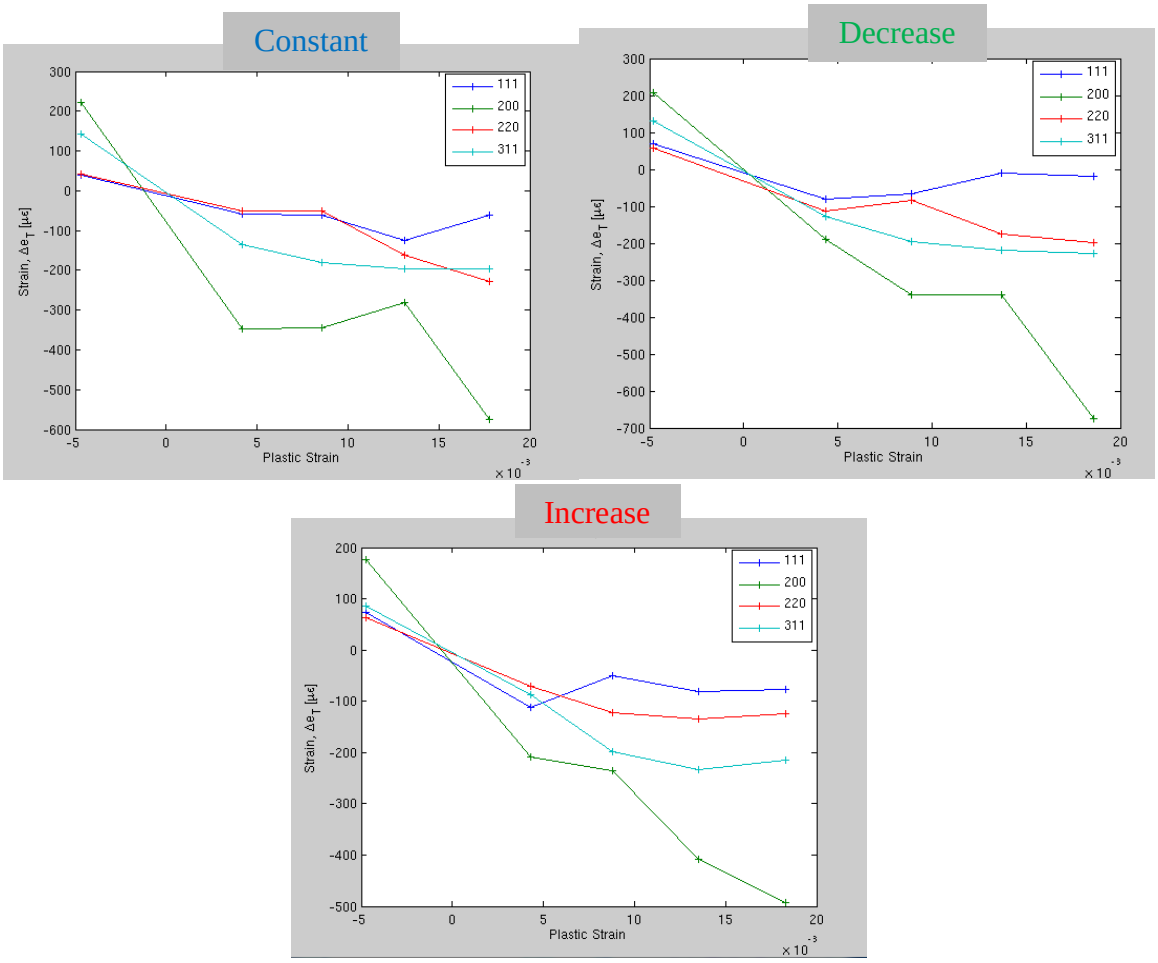

Figure 16: Diffraction plots of internal grains for the same cases.

Interestingly, however, the FWHM of the sample is more consistent from case to case. The trend is similar between the total and internal grains (shown in Figure 17). The only variation is that each diffraction group, most notably the soft ⟨200⟩ group, has a smaller standard deviation when there are more data present. This is intriguing, because it

indicates that the external grains have a more narrow distribution of FWHM, and thus less heterogeneity.

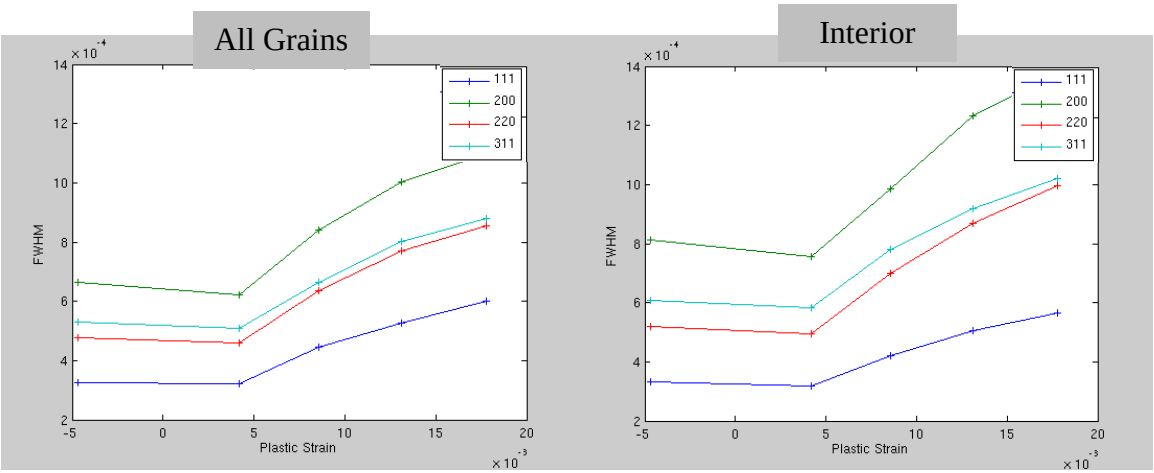

Figure 17: FWHM plots of all grains and internal grains for the constant case, for comparison. The remaining cases can be seen in the appendix.

A comparison of diffraction behavior in precompressed samples compared to purely tension samples would be useful to determine the samples behavior in future tests. Figure 18 shows the diffraction behavior, and Figure 19 the FWHM.

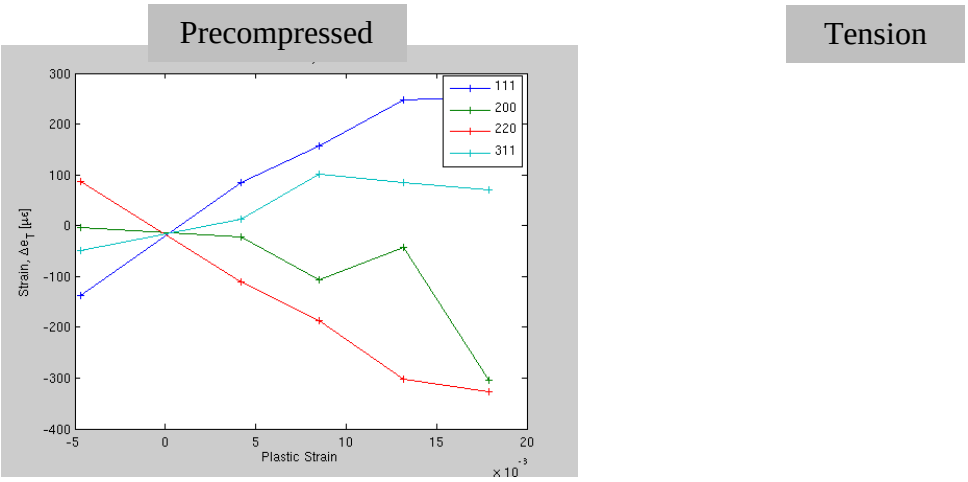

Figure 18: Diffraction plots of compression compared to tension. Average displacement seems to be greater in the precompressed case, but since this is unaveraged, the trend likely differs on the macro level.

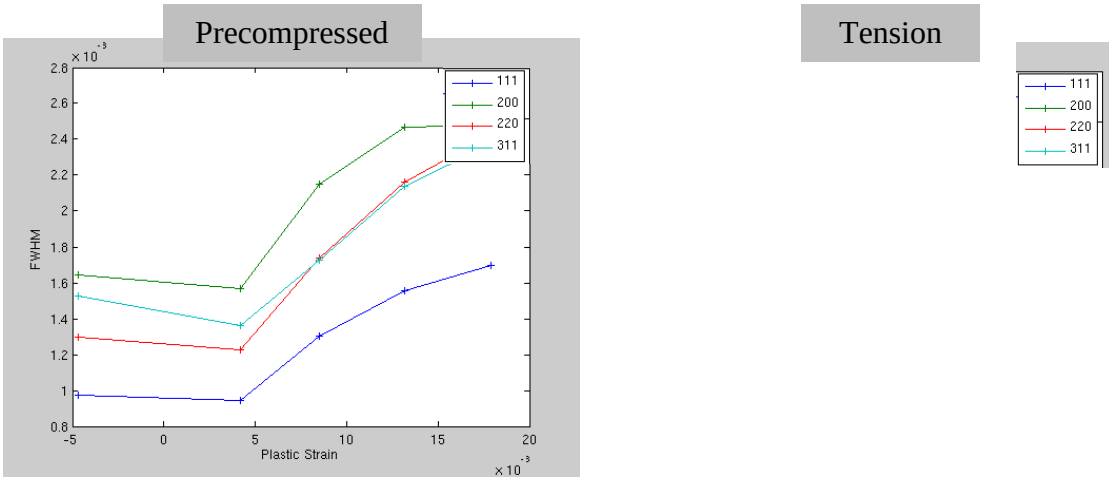

Figure 19: Diffraction plots of compression compared to tension. Average displacement seems to be greater in the precompressed case, but since this is unaveraged, the trend likely differs on the macro level.

The FWHM behavior matches that of experiments, and unaveraged, FWHM would likely be the best route to determine how any large change in τ_C affects behavior

CHAPTER 4: CONCLUSIONS AND FUTURE TESTING

Conclusions

While not perhaps confirming a specific hardening or softening relation in Nanocrystalline Ni, it is possible to rule out hardening and any significant change to the population of locally soft and hard grains within the model. Hardening as a whole creates a more symmetric τ_C distribution, negatively impacting the hysteretic strain width, thus, large amounts of strain are not reasonable for this model. A more modest hardening, around 1% increase per slip event, would be acceptable, but not confirmed. Softening behavior also negatively affects reversible plasticity, but generally the model has to be pushed to its limit to show any behavioral changes.

In terms of diffraction data, a larger data set is necessary in order to create a statistically significant trend in diffraction peak displacement, and the FWHM of the material would be a good parameter to monitor extreme cases in order to benefit. The FWHM does show promise for comparison to experimental data because of its consistency.

Future Testing

There are several general directions I see this model eventually heading. The most logical extension at this moment is to complete the diffraction simulations with completely random sets of Euler angles, rather than shuffling the same angle sets around. A cyclic test without precompression could be used to compare the diffraction data FWHM, to see if the averages are affected by the precompression. Additionally, creating unloading/loading points at 0.00 plastic strain is imperative in order to fully understand qualitatively the shape of the diffraction curves, so that the mo

Recent diffraction data from Sun et al. indicate that steady-state creep is a new area to explore, and that there are competing processes within NC materials. A modification of the variation to include time-dependent change in τ_C could help us improve the current model, and create a quantitative understanding of the competing mechanism proposed in the literature [7].

A second expansion of this model should include having a separate value of τ_C for each slip system, to try to solve the issue of a minimum. This would make the model similar to Yuan et al., but may require a new τ_C distribution to fit the static critical resolved shear stress case [8].

REFERENCES

[1] L. Li, S. Van Petegem, H. Van Swygenhoven, P.M. Anderson. Slip-induced intergranular stress redistribution in nanocrystalline Ni, Acta Materialia 60 (2012) 7001-7010.

[2] L. Li. A quantized crystal plasticity model for nanocrystalline metals: Connecting atomistic simulations and physical experiments. Materials Science and Engineering, vol. Doctor of Philosophy. Columbus, Ohio: The Ohio State University, 2011. p.156.

[3] L. Li, P.M. Anderson, M.G. Lee, E. Bitzek, P. Derlet, H. Van Swygenhoven. The stress-strain response of nanocrystalline metals: A quantized crystal plasticity approach, Acta Materialia 57 (2009) 812-822.

[4] M.A. Meyers, A. Mishra, D.J. Benson. The deformation physics of nanocrystalline metals: Experiments, analysis, and computations, Jom 58 (2006) 41-48.

[5] H. Gleiter. NANOCRYSTALLINE MATERIALS, Progress in Materials Science 33 (1989) 223-315.

[6] D. Wolf, V. Yamakov, S.R. Phillpot, A. Mukherjee, H. Gleiter. Deformation of nanocrystalline materials by molecular-dynamics simulation: relationship to experiments?, Acta Materialia 53 (2005) 1-40.

[7] Z. Sun, S. Van Petegem, A. Cervellino, K. Durst, W. Blum, H. Van Swygenhoven. Dynamic recovery in nanocrystalline Ni, Acta Materialia 91 (2015) 91-100.

[8] R. Yuan, I.J. Beyerlein, C.Z. Zhou. Emergence of grain-size effects in nanocrystalline metals from statistical activation of discrete dislocation sources, Acta Materialia 90 (2015) 169-181.

[9] M. Dao, L. Lu, R.J. Asaro, J.T.M. De Hosson, E. Ma. Toward a quantitative understanding of mechanical behavior of nanocrystalline metals, Acta Materialia 55 (2007) 4041-4065.

[10] P.M. Anderson, J.S. Carpenter, M.D. Gram, L. Li. Mechanical Properties of Nanostructured Metals. in: Bhushan B, Luo D, Schricker SR, Sigmund W, Zauscher S, (Eds.). Handbook of Nanomaterials Properties. Springer-Verlag Berlin Heidelberg, 2014. pp. 495-553.

[11] L. Li, P.M. Anderson. Quantized Crystal Plasticity Modeling of Nanocrystalline Metals. in: Weinberger CR, Garritt J, (Ed.). Multiscale Materials Modeling for Nanomechanics. Springer International Publishing, 2016.

[12] E. Bitzek, P.M. Derlet, P.M. Anderson, H. Van Swygenhoven. The stress-strain response of nanocrystalline metals: A statistical analysis of atomistic simulations, Acta Materialia 56 (2008) 4846-4857.

[13] H.H. Fu, D.J. Benson, M.A. Meyers. Analytical and computational description of effect of grain size on yield stress of metals, Acta Materialia 49 (2001) 2567-2582.

[14] Y.J. Wei, C. Su, L. Anand. A computational study of the mechanical behavior of nanocrystalline fcc metals, Acta Materialia 54 (2006) 3177-3190.

[15] B. Zhu, R.J. Asaro, P. Krysl, K. Zhang, J.R. Weertman. Effects of grain size distribution on the mechanical response of nanocrystalline metals: Part II, Acta Materialia 54 (2006) 3307-3320.
[16] R.J. Asaro, S. Suresh. Mechanistic models for the activation volume and rate sensitivity in metals with nanocrystalline grains and nano-scale twins, Acta Materialia 53 (2005) 3369-3382.
[17] Y.J. Wei, A.F. Bower, H.J. Gao. Recoverable creep deformation due to heterogeneous grain-boundary diffusion and sliding, Scripta Materialia 57 (2007) 933-936.
[18] D. Peirce, R.J. Asaro, A. Needleman. AN ANALYSIS OF NONUNIFORM AND LOCALIZED DEFORMATION IN DUCTILE SINGLE-CRYSTALS, Acta Metallurgica 30 (1982) 1087-1119.
[19] R.J. Asaro, A. Needleman. OVERVIEW .42. TEXTURE DEVELOPMENT AND STRAIN-HARDENING IN RATE DEPENDENT POLYCRYSTALS, Acta Metallurgica 33 (1985) 923-953.
[20] L. Li, M.G. Lee, P.M. Anderson. Critical Strengths for Slip Events in Nanocrystalline Metals: Predictions of Quantized Crystal Plasticity Simulations, Metallurgical and Materials Transactions a-Physical Metallurgy and Materials Science 42A (2011) 3875-3882.
[21] S.R. Kalidindi, C.A. Bronkhorst, L. Anand. CRYSTALLOGRAPHIC TEXTURE EVOLUTION IN BULK DEFORMATION PROCESSING OF FCC METALS, Journal of the Mechanics and Physics of Solids 40 (1992) 537-569.
[22] H.B. Huntington. The Elastic Constants of Crystals, Academic Press, New York, 1958.
[23] Abaqus. Abaqus Documentation. vol. 6.13. Providence, RI, USA: Dassault Systèmes, 2013.
[24] L. Li, P. Christodoulou, P. Anderson. A Quantized Crystal Plasticity Model for Nanocrystalline Metals: Connecting Atomistic Simulations and Physical Experiments. TMS Annual Meeting & Exhibition. Nashville, TN, 2016.

APPENDIX

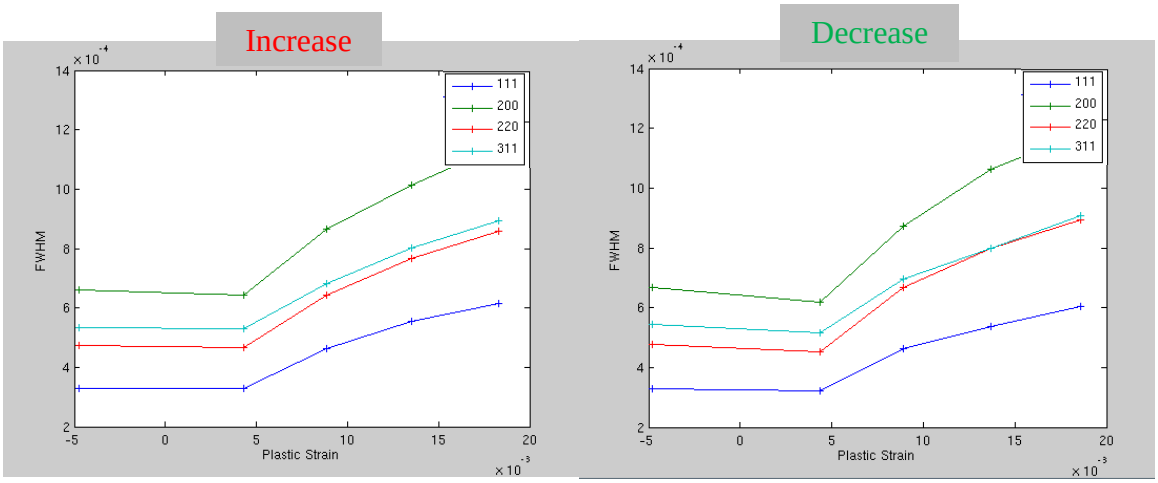

Figure 20: FWHM plots of all grains for the increased (1%) case and decreased (10%) τ_C, for comparison.

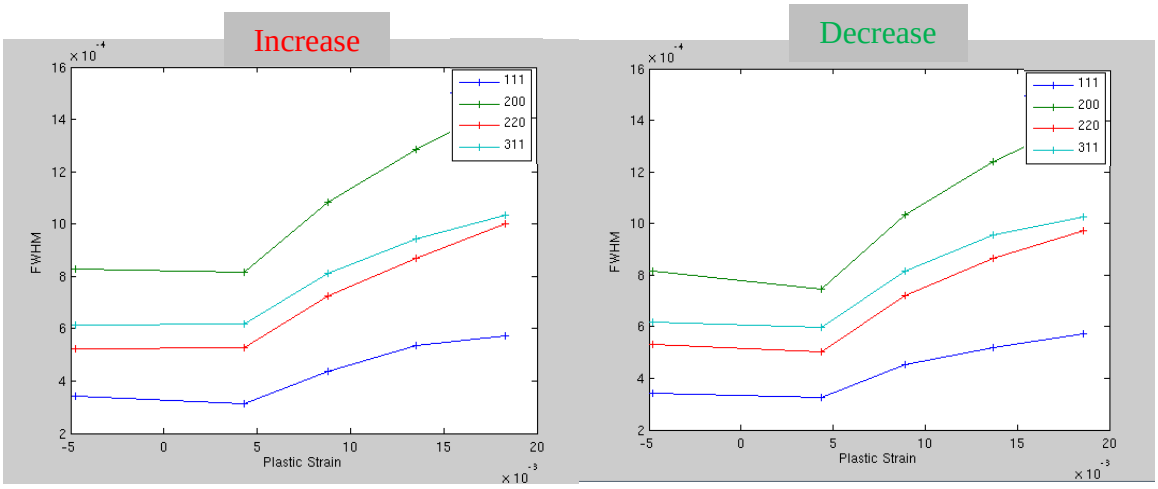

Figure 21: FWHM plots of all grains for the increased (1%) case and decreased (10%) τ_C, for comparison.